Report

Current Biology

Lamin Mutations Accelerate Aging via Defective Export of Mitochondrial mRNAs through Nuclear Envelope Budding

Highlights

- Mitochondrial RNAs, such as mitofusin, localize to nuclear envelope budding sites
- A fly model of progeroid syndrome caused by A-type lamin mutation ages prematurely
- Aging phenotypes include mitochondrial degeneration and mitofusin RNA depletion
- Accelerated aging phenotypes are preceded by a block of nuclear envelope budding

Authors

Yihang Li, Linda Hassinger, Travis Thomson, Baojin Ding, James Ashley, William Hassinger, Vivian Budnik

Correspondence

vivian.budnik@umassmed.edu

In Brief

Li et al. link the nuclear envelope (NE)-budding export pathway to premature aging in fly models of progeroid syndromes induced by A-type lamin mutations. They find mitochondrial RNAs, such as mitofusin, at NE-budding sites and show that disruption of NE budding prior to adulthood results in accelerated aging and mitochondrial degeneration in adults.

Li et al., 2016, Current Biology *26*, 1–8
August 8, 2016
http://dx.doi.org/10.1016/j.cub.2016.06.007

CellPress

Please cite this article in press as: Li et al., Lamin Mutations Accelerate Aging via Defective Export of Mitochondrial mRNAs through Nuclear Envelope Budding, Current Biology (2016), http://dx.doi.org/10.1016/j.cub.2016.06.007

Current Biology
Report

Lamin Mutations Accelerate Aging via Defective Export of Mitochondrial mRNAs through Nuclear Envelope Budding

Yihang Li,[1] Linda Hassinger,[1] Travis Thomson,[1] Baojin Ding,[1] James Ashley,[1] William Hassinger,[1] and Vivian Budnik[1,*]
[1]Department of Neurobiology, University of Massachusetts Medical School, Worcester, MA 01655, USA
*Correspondence: vivian.budnik@umassmed.edu
http://dx.doi.org/10.1016/j.cub.2016.06.007

SUMMARY

Defective RNA metabolism and transport are implicated in aging and degeneration [1, 2], but the underlying mechanisms remain poorly understood. A prevalent feature of aging is mitochondrial deterioration [3]. Here, we link a novel mechanism for RNA export through nuclear envelope (NE) budding [4, 5] that requires A-type lamin, an inner nuclear membrane-associated protein, to accelerated aging observed in *Drosophila* LaminC (LamC) mutations. These LamC mutations were modeled after A-lamin (LMNA) mutations causing progeroid syndromes (PSs) in humans. We identified mitochondrial assembly regulatory factor (Marf), a mitochondrial fusion factor (mitofusin), as well as other transcripts required for mitochondrial integrity and function, in a screen for RNAs that exit the nucleus through NE budding. PS-modeled LamC mutations induced premature aging in adult flight muscles, including decreased levels of specific mitochondrial protein transcripts (RNA) and progressive mitochondrial degradation. PS-modeled LamC mutations also induced the accelerated appearance of other phenotypes associated with aging, including a progressive accumulation of polyubiquitin aggregates [6, 7] and myofibril disorganization [8, 9]. Consistent with these observations, the mutants had progressive jumping and flight defects. Downregulating *marf* alone induced the above aging defects. Nevertheless, restoring *marf* was insufficient for rescuing the aging phenotypes in PS-modeled LamC mutations, as other mitochondrial RNAs are affected by inhibition of NE budding. Analysis of NE budding in dominant and recessive PS-modeled LamC mutations suggests a mechanism by which abnormal lamina organization prevents the egress of these RNAs via NE budding. These studies connect defects in RNA export through NE budding to progressive loss of mitochondrial integrity and premature aging.

RESULTS AND DISCUSSION

Mitochondrial RNAs Localize to NE-Budding Sites

Nuclear envelope (NE) budding is a mechanism for the nuclear export of large ribonucleoprotein granules (megaRNPs) [4]. This mechanism is akin to the nuclear egress of herpes-type viruses [10] and involves megaRNP envelopment at the inner nuclear membrane (INM) and RNP de-envelopment at the outer nuclear membrane (ONM). Sites of NE budding in *Drosophila* larval muscle nuclei are identified by using antibodies to the C-terminal fragment of DFrizzled2 (DFz2C), which associates with megaRNPs, and by the presence of locally thickened NE with brighter LamC immunoreactivity (DFz2C/LamC foci) [4, 11]. These DFz2C/LamC foci are enriched in RNAs encoding for several postsynaptic proteins [4, 12]. Fluorescence in situ hybridization (FISH) demonstrated that a subset of LamC foci also contained *marf* RNA (Figures 1A, S1A, and S1B), implicating NE budding in the export of mitochondria-related transcripts. RNA immunoprecipitation (RIP) from larval muscles using anti-DFz2C established that *marf* RNA, but not the unrelated *mad* RNA [4], co-precipitated with DFz2C, consistent with its presence in megaRNPs (Figure 1B).

To determine whether other mitochondria-associated RNAs existed in megaRNPs, we performed FISH to detect ATP-synthase (ATP-syn) subunits, the electron-transport chain component COX4, the kinase PINK1, and the mitochondrial fission factor Drp1. *ATP-syn-*β, *-*α (*Bellwether/Blw*), and *-B* RNAs were enriched at NE-LamC foci, suggesting their presence in megaRNPs (Figures 1C–1E and S1C–S1E). FISH signal for *ATP-syn-*γ, *-C*, and *Drp1* was very low (not shown) and undetected for *cox4* and *pink1* (Figures 1F and 1G). Thus, only a subset of mitochondria-associated transcripts is present within megaRNPs.

PS-Modeled LamC Mutations Display Age-Dependent Mitochondrial Defects

Marf, a guanosine triphosphatase (GTPase) of the mitofusin family, is involved in mitochondrial fusion, a process essential for maintaining mitochondrial integrity and respiratory function [13]. Similarly, ATP-synthase is required for the formation and maintenance of mitochondrial cristae [14]. As aging and neurodegenerative disorders have been linked to progressive mitochondrial disruption [8, 15], we examined mitochondria in flies expressing progeroid syndrome (PS)-modeled LamC mutations. These LamC variants contained point mutations in conserved

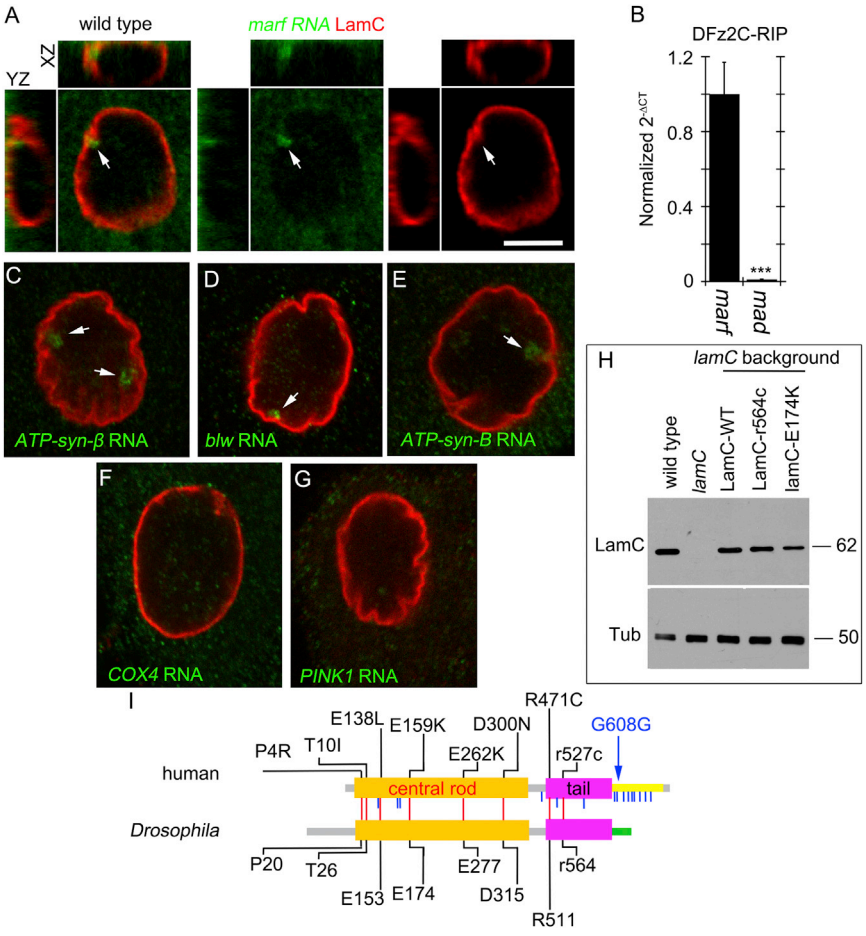

Figure 1. Association of *marf* mRNA with DFz2C and Nuclear LamC Foci

(A and C–G) FISH of a larval body wall muscle preparations using a (A) *marf*, (C) *ATP-syn-β*, (D) *blw*, (E) ATP-syn-B, (F) *cox4*, and (G) *pink1* DNA probe and antibodies to LamC. Arrows denote foci containing mitochondrial transcripts.

(B) Real-time PCR of *marf* and *mad* after RNA immunoprecipitation with DFz2C antibody from larval body wall muscles.

(H) Western blot of body wall muscle protein extracts from animals of the indicated genotypes probed with antibodies to LamC (top) and tubulin (Tub; bottom). Numbers at the right represent molecular weight in KDa.

(I) Schematic depiction of *Drosophila* LamC and human LMNA protein structure, indicating conserved (red vertical lines) and non-conserved (blue vertical lines) amino acid residues that, when mutated, cause progeroid syndromes in humans. Blue arrow indicates the mutation responsible for most HGPS cases.

***p < 0.001; error bars = SEM. Scale bar, 6 μm in (A) and (C)–(G). See also Figure S1.

amino acid codons that, in human *LMNA*, gave rise to PS (Figure 1I). We focused on LamC-E174K (E159K in LMNA) and LamC-R564C (R527C in LMNA; referred to as LamC-r564c to denote recessive inheritance) in the rod and tail domains of LamC (Figure 1I). We also generated flies expressing wild-type LamC (LamC-WT). In humans, LMNA-E159K is an autosomal-dominant mutation causing atypical PS with a presentation similar to Hutchinson-Gilford progeria syndrome (HGPS) [16]. LMNA-r527c is an autosomal-recessive mutation inducing atypical HGPS [17]. Western blots of body wall muscle proteins from *lamC*-null mutants expressing LamC variants with myosin heavy chain (MHC)-Gal4 revealed that the transgenes were expressed in the same range as WT (Figure 1H). Because LMNA-E159K behaves as a dominant mutation in humans, LamC-E174K was expressed in a *lamC*/+ heterozygous background (genotype: LamC-E174K, *lamC*/+). Because LMNA-r527c is a recessive mutation in humans, LamC-r564c was expressed in a *lamC* mutant homozygous background (genotype: LamC-r564c, *lamC*/*lamC*).

We focused on adult dorsal longitudinal muscles (DLM) of the indirect flight muscles, because larval muscles are short-lived, precluding aging studies [18]. We examined mitochondria using antibodies against mammalian ATP-syn-α, which cross-react with Blw [19], in young (3-day posteclosion [3d]) and middle age (14d and 21d) adults.

In WT and LamC-WT, anti-ATP-syn-α labeled elongated mitochondria located above and below myofibrils at all stages (Figures 2A, 2B, 2D, 2E, 2G, and 2H), which was similar to 3d LamC-E174K (Figure 2C). In 14d and 21d LamC-E174K, however, mitochondria were smaller, appeared rounded, and were sparse (Figures 2F and 2I). This was reflected by a significant reduction of mitochondrial volume (Figure 2J), suggesting an age-dependent decline in mitochondria production and/or maintenance. *lamC*-null mutants did not survive to adulthood, precluding the examination of animals expressing LamC-r564c.

These mitochondrial phenotypes and the presence of *marf* RNA in megaRNPs raised the possibility that age-dependent mitochondrial deterioration could be partially attributed to defective Marf levels. Indeed, *marf* RNA was markedly depleted in thoracic muscles from 21d LamC-E174K, compared to 21d controls and LamC-WT (Figure 2K).

At the ultrastructural level, in 4d and 21d controls, mitochondria were packed between myofibrils, which were maintained even in 60d animals (Figures 3A, S2A1, and S2D1). This was similar to 4d and 21d LamC-WT (Figures S2B1 and S2E1) and 4d LamC-E174K (Figure S2C1). Additionally, mitochondrial cristae appeared normal (Figures 3A, S2A2, S2B2, S2D2, and S2E2). Instead, 14d and 21d LamC-E174K animals exhibited swollen mitochondria (Figures 3B and 3C) with collapsing or disintegrating cristae (Figures 3B and 3C). This was reflected in a significant reduction in mitochondria electron density (Figure S2F). Closer examination already revealed subtle abnormalities in 4d LamC-E174K animals (Figure S2C2).

Expression of Marf-RNAi in DLMs also elicited dramatic mitochondrial aberrations (Figures 3D, 3E, and S2F). However, overexpressing Marf in the DLM of LamC-E174K, *lamC*/+ animals was insufficient to rescue mitochondrial defects (Figures 2J, 2L, 3G, and S2F). Thus, Marf is not the only mitochondrial factor involved in maintaining mitochondrial integrity in PS-LamC

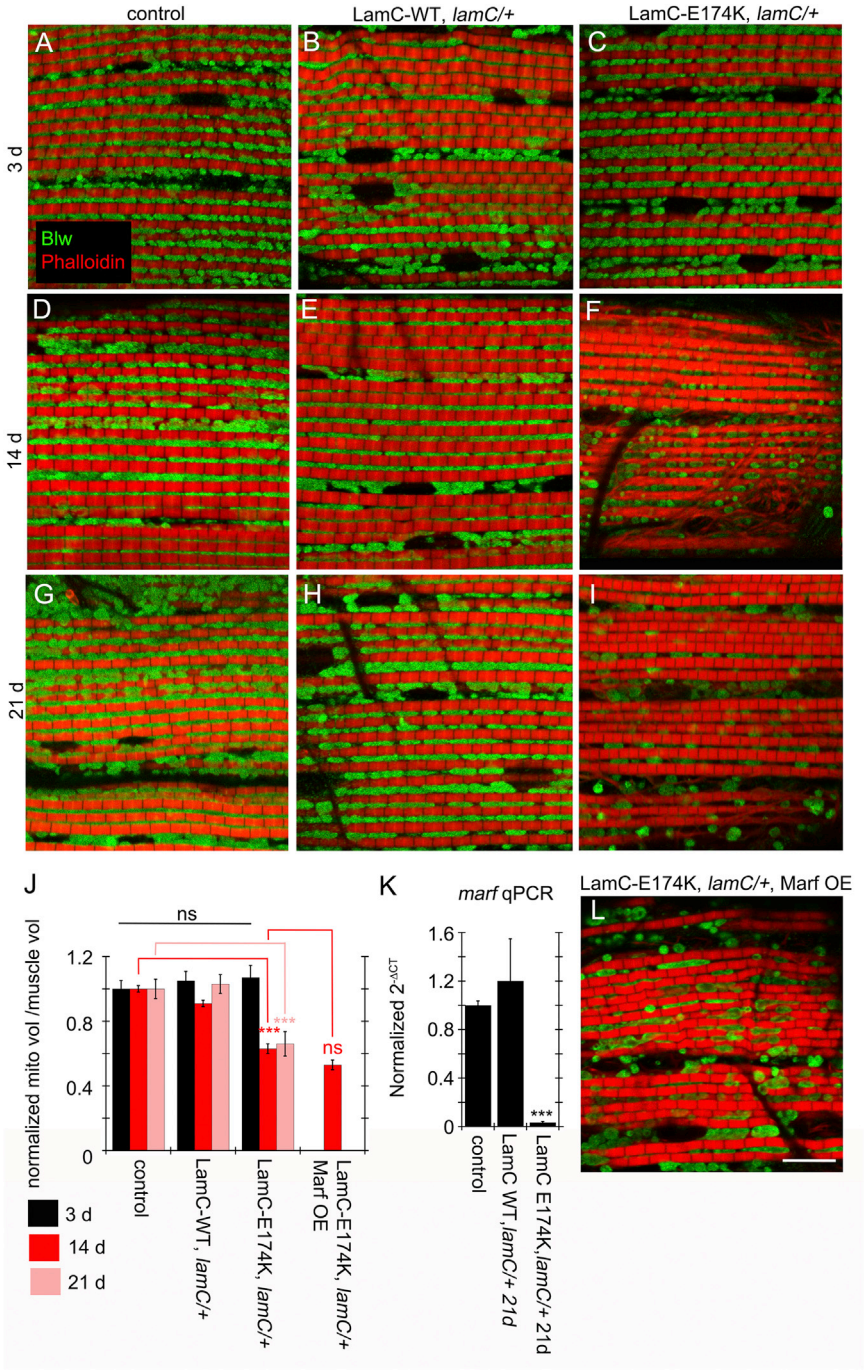

Figure 2. Age-Dependent Alterations in Adult-Muscle Mitochondria upon Expressing LamC-E174K

(A–I and L) DLMs labeled with anti-ATP-syn-α and rhodamine-conjugated phalloidin from (A–C) 3-, (D–F and L) 14-, and (G–I) 21-day-old (A, D, and G) MHC-Gal4 control; (B, E, and H) LamC-WT, *lamC*/+; (C, F, and I) LamC-E174K, *lamC*/+; and (L) LamC-E174K, lamC/+, Marf OE.

(J) Quantification of mitochondrial volume normalized to muscle volume.

(K) Real-time PCR of *marf* RNA levels in adult thoracic muscle from the indicated genotypes.

n (left to right) = (J): 30, 49, and 28; 35, 33, and 31; 28, 47, and 32; 36. ***p < 0.001; error bars = SEM. Scale bar, 9 μm.

mutations. Indeed, downregulating the megaRNP component, Blw, also elicited mitochondrial defects (Figures 3F and S2F).

To determine whether the mitochondrial phenotypes resulted from defective NE budding and not nuclear pore complex (NPC)-mediated export [20], we expressed DFz2-dominant-negative (DFz2-DN) [21], a LamC-independent method to block NE budding. This induced mitochondrial disruption, including sparse and collapsed cristae (Figures 3H and S2F).

We also observed progressive defects in muscle fibers in LamC-E174K animals. In contrast to controls, LamC-WT, and 4d LamCE174K (Figures S3A–S3E), 21d LamCE174K animals exhibited thinner myofibrils, sarcomere disorganization, and vanishing Z lines and A bands (Figure S3F), consistent with the sarcopenia observed in very old WT flies. This phenotype was mimicked by expressing Marf-RNAi in DLMs (Figure S3G).

PS-Modeled LamC Mutations Display Additional Signs of Aging

An aging marker is a decline in protein quality control, resulting in accumulation of polyubiquitinated protein aggregates [6, 7]. In 3d, 14d, and 21d-old WT flies, we observed no polyubiquitin aggregates in DLMs (Figures S3H, S3I, and S3K), but these were abundant in 60-day-old flies (Figures S3J and S3K).

DLMs from 3d LamC-WT or LamC-E174K flies were devoid of polyubiquitin aggregates (Figures 3I, 3J, and 3O). However, numerous polyubiquitin aggregates were observed in 14d LamC-E174K, but not LamC-WT flies (Figures 3K, 3L, and 3P). Thus, LamC-E174K animals display accelerated defects in proteostasis, as in normal aging. Downregulating Marf in muscle also led to early appearance of polyubiquitin aggregates (Figures 3M and 3P), and overexpressing Marf in LamC-E174K DLMs partially rescued levels of polyubiquitin aggregates (Figures 3N and 3P). Given that expressing LamC-E174K leads to a reduction in Marf, and that downregulating Marf alone mimics LamC-E174K phenotypes, these results provide compelling evidence for a primary role of Marf in sustaining mitochondrial integrity, normal muscle mass, and proteostasis. Lack of proper mitochondrial replenishment leads to reactive oxygen species (ROS) accumulation in mitochondria derived from oxidative metabolism, inducing cellular damage. Indeed, HGPS patients display an increase in ROS, altered energy generation, and elevated genomic

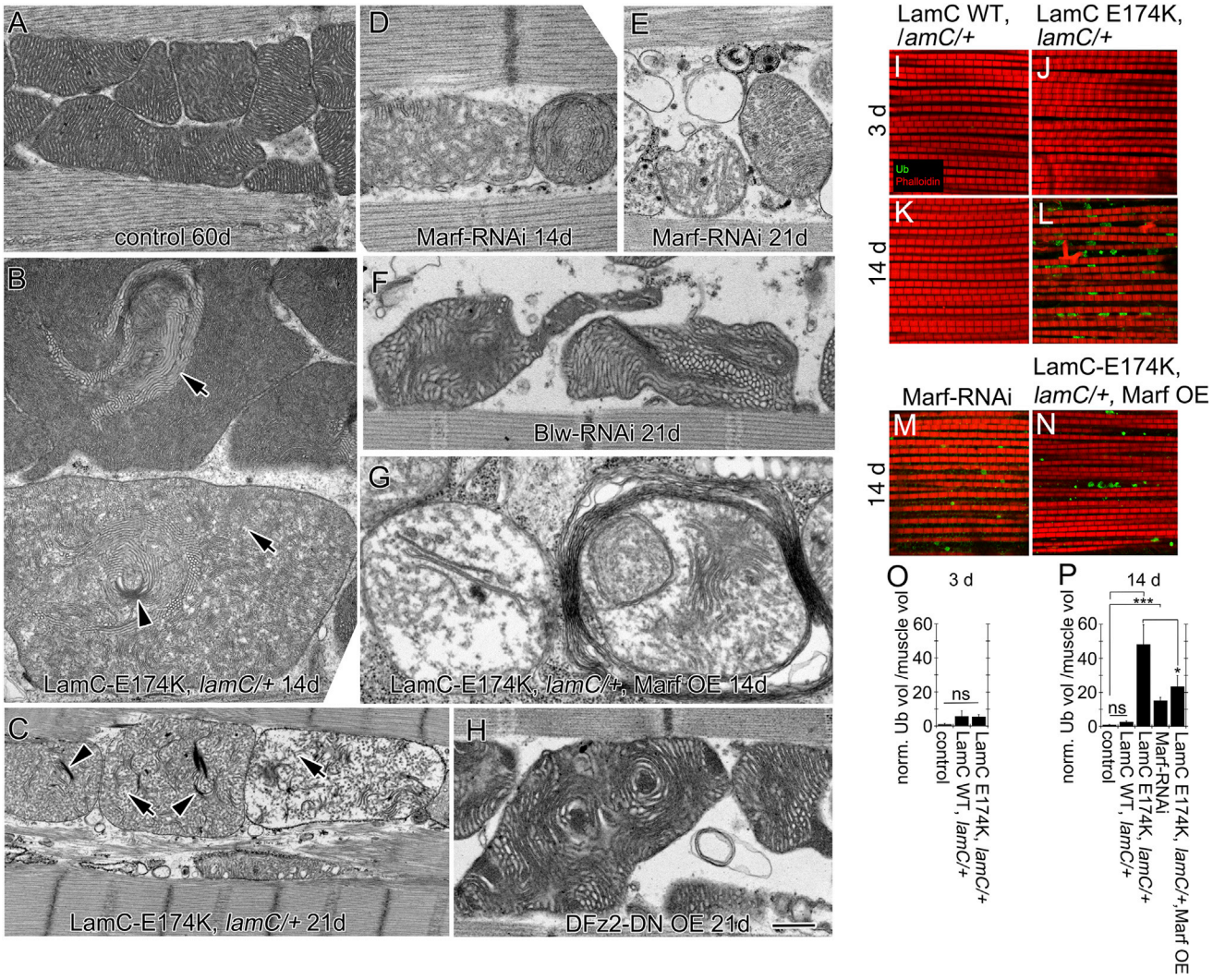

Figure 3. Disruption of Adult-Muscle Mitochondria and Progressive Polyubiquitin Aggregate Accumulation upon Expressing LamC-E174K

(A–H) EM micrographs of adult DLMs showing mitochondrial cristae structure in (A) 60-day, (B, D, and G) 14-, and (C, E, F, and H) 21-day-old flies of the following genotypes: (A) MHC-Gal4/+; (B and C) LamC-E174K, *lamC*/+; (D and E) Marf-RNAi-muscle; (F) Blw-RNAi-muscle; (G) lamC-E174K, *lamC*/+ Marf OE; and (H) DFz2-DN OE muscle. Arrowheads denote collapsing cristae; arrows denote disintegrating cristae.

(I–N) DLMs double-labeled anti-ubiquitin and rhodamine-conjugated phalloidin in (I and J) 3- and (K–N) 14-day-old adults from (I and K) LamC-WT, *lamC*/+; (J and L) LamC-E174K, *lamC*/+; (M) Marf-RNAi-muscle; and (N) LamC-E174K, *lamC*/+ Marf OE.

(O and P) Quantification of ubiquitin aggregate volume normalized to muscle volume.

n (left to right) = (O) 29, 30, and 29 and (P) 85, 30, 35, 36, and 36. *$p < 0.05$; ***$p < 0.001$; error bars = SEM. Scale bar, 0.5 μm in (A), (B), and (H); 0.4 μm for (D)–(G); 1 μm for (C); and 16 μm for (I)–(N). See also Figures S2 and S3.

instability markers [22]. Our studies raise the possibility that at least some of the defects observed in PS are derived from abnormal transport of RNAs that are required to sustain mitochondrial replenishment.

Mitochondrial replenishment is based on an equilibrium among mitochondrial fusion, fission, and autophagy. Balanced mitochondrial fusion and fission restores damaged mitochondrial compartments, whereas excessive fission leads to fragmentation followed by autophagy to dispose of damaged mitochondria. Studies suggest that normal aging is accompanied by a shift toward fission and decreased fusion [23]. Our studies indicate that a decrease in mitochondrial fusion might result from abnormal RNA export in PS-modeled mutations. Interestingly, we found that LamC-E174K induced a decrease in *marf*, accompanied by accelerated disruption of mitochondria. As *marf* RNA is a component of megaRNPs and LamC-E174K disrupts NE budding (see below), these observations are consistent with a role of NE budding in the export of mitochondrial factors required for normal aging.

MegaRNPs have been associated with developmental periods characterized by high-protein synthesis demand, such as after fertilization of the mammalian oocyte and during the rapid expansion of the fly larval neuromuscular junction (NMJ). Interestingly, *marf* RNA expression is moderate throughout

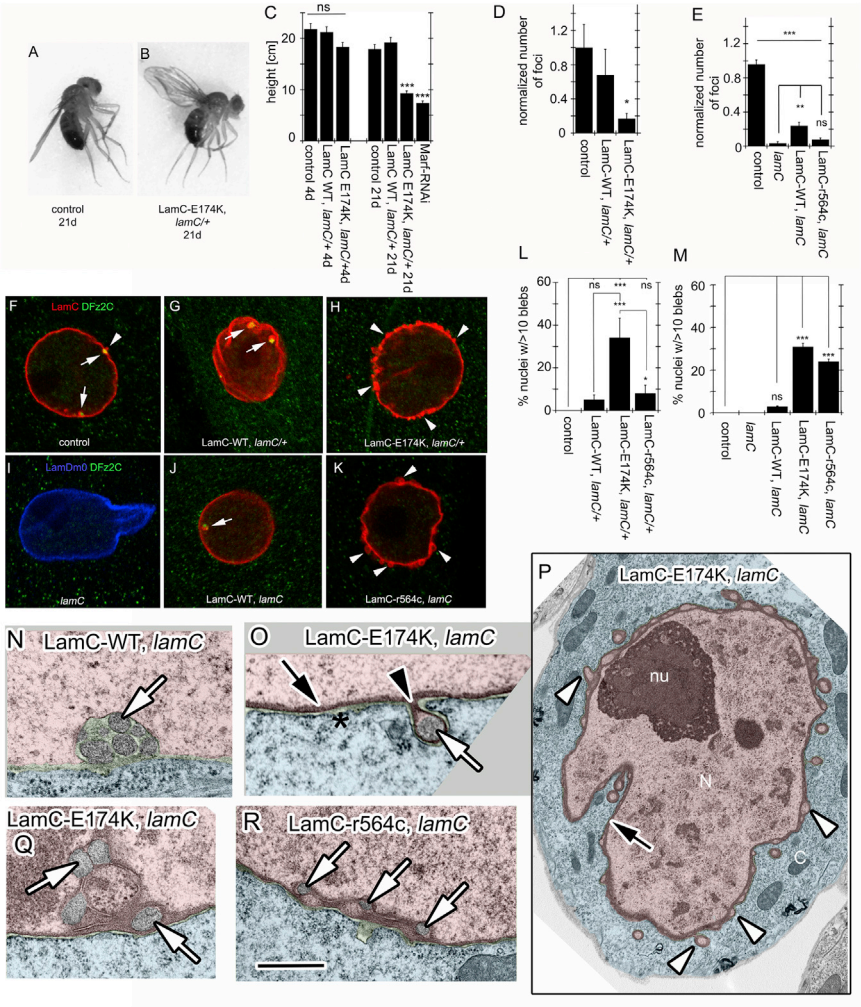

Figure 4. Expression of PS-Modeled Mutations Disrupts NE Morphology and Ultrastructure

(A and B) Wing position in (A) control flies, showing normal wing position, and (B) LamC-E174K, *lamC*/+ flies, showing a "wings-up" phenotype.

(C) Quantification of landing height in 4- and 21-day-old adults.

(D and E) Quantification of the number of DFz2C/LamC foci at body wall muscles normalized to BG487/+ controls in the indicated genotypes in a (D) *lamC*/+ or (E) *lamC*-null mutant background.

(F–K) Larval body wall muscle nuclei labeled with anti-LamC or anti-LamDm0 and anti-DFz2C antibody from (F) BG487-Gal4/+ control; (G) LamC-WT, *lamC*/+ (arrows denote LamC/DFz2C foci; arrowheads denote abnormal LamC blebs); (H) LamC-E174K, *lamC*/+; (I) *lamC*-null mutant; (J) LamC-WT, *lamC*; and (K) LamC-r564c, *lamC*. Arrows point to DFz2C/LamC foci and arrowheads to blebs.

(L and M) Quantification of the percentage of body wall muscle nuclei containing more than ten blebs at the NE in the indicated genotypes (L) in a *lamC*/+ heterozygous background and (M) in a *lamC*-null mutant background. Control is BG487/+ in both graphs.

(N–R) Transmission EM (TEM) of larval body wall muscle nuclei from (N) LamC-WT, *lamC*; (O–Q) LamC-E174K, *lamC*; and (R) LamC-r564c, *lamC*. White arrows denote megaRNP granules, white arrowheads denote empty blebs, black arrows denote thickened lamina, and black arrowheads denote thickened lamina at the neck of blebs.

*p < 0.05; **p < 0.01; ***p < 0.001; error bars = SEM. n (left to right) = (C) 81, 78, 83, 166, 83, 85, and 89 and (D, E, L, and M; number of hemisegments/number of nuclei) (D) 21/1,137, 21/1,026, and 24/1,248; (E) 17/958, 13/666, 17/951, and 19/977; (L) 20/1,155, 20/1,106, 20/1,035, and 12/647; (M) 26/1,500, 14/720, 23/1,274, 19/1,079, and 16/829. Scale bar, 5.5 μm for (F)–(K), 1.4 μm for (P), and 0.4 μm for (N), (O), (Q), and (R). See also Figure S4.

development, with a peak near the end of embryogenesis, and a very large peak in the young adult, starting at late pupariation and increasing into early adulthood (http://flybase.org/reports/FBgn0029870.html). The progressive deterioration of muscles and mitochondria observed in PS-modeled adults is consistent with a gradual run down of mitochondrial components needed to be maintained at high levels in the adult. Flight-muscle function imposes great energy demands, making it likely that mitochondria in flight muscles require continuous replenishment. It is thus conceivable that NE budding serves to provide an early pool of the RNAs required to sustain this replenishment and that blocking NE budding dramatically decreases the size of this early pool. In turn, this leads to early aging, due at least in part to an inability to restore mitochondrial function, and thus the damaging effects of increased ROS.

LamC-E174K Expression Disrupts Flight Behavior

The abnormalities in middle age LamC-E174K DLMs were reflected in flight and wing-position defects. Unlike WT, LamC-WT, and young LamC-E174K flies (Figure 4A), 21d LamC-E174K animals had a "wings up" wing position (Figure 4B). Also, 21d LamC-E174K failed to jump or fly, as determined in a flight assay [24] conducted within an oil-coated cylinder. WT, LamC-WT, and 3d LamC-E174K flies jump and fly when startled, becoming stuck at various heights of the cylinder walls (Figure 4C; Movies S1 and S2). 21d LamC-E174K showed about a 50% decrease in landing height (Figure 4C), resulting from an inability to jump and fly (Movie S2). Consistent with a role of Marf in the above defect, Marf downregulation in muscles also elicited similar behavioral defects (Figure 4C).

PS-Modeled LamC Mutations Have Defective NE Budding

The observations above raised the possibility that defects in NE budding could be linked to accelerated aging. Thus, we determined whether PS-modeled LamC mutations elicited NE-budding defects prior to the aging defects, using three readouts: the presence of nuclear DFz2C/LamC foci, megaRNP granules at the perinuclear space, and the development of the

larval NMJ, whose growth and maturation require the export of certain postsynaptic RNAs through NE budding [4, 11].

LamC-WT larval muscle nuclei contained DFz2C/LamC foci that were similar to controls in appearance and number (Figures 4D, 4F, and 4G, arrows). In contrast, nuclei in LamC-E174K larvae displayed dramatic decrease in DFz2C/LamC foci (Figures 4D and 4H). Instead, the lamina exhibited numerous small blebs, which, except for rare occasions, were devoid of DFz2C (Figures 4H and 4L, arrowheads, and S4A). Such blebs are observed in WT at a very low frequency (Figure 4F, arrowhead). Consistent with LamC-r564c behaving as a recessive mutation, LamC-r564c, *lamC*/+ heterozygotes did not display the above phenotypes (Figure 4L). Nevertheless, when expressed in a *lamC*-null background, LamC-r564c showed a significant decrease in DFz2C/LamC foci (Figures 4E and 4K) and a copious increase in nuclear blebs (Figures 4K, 4M, S4B, and S4C). Blebs were not observed in controls, *lamC* nulls, or LamC-WT (Figures 4I, 4J, and 4M). Similar lamina blebs were observed in *Drosophila* Schneider-2 (S2) cells upon induction of LamC variant expression (Figures S4D–S4F). The disruption of DFz2C/LamC foci formation suggests defective NE budding in PS-LamC mutations.

At the ultrastructural level, megaRNPs in control and LamC-WT cells/muscles were observed at the NE either as single (Figure S4G) or clustered electron dense granule(s) at the perinuclear space (Figure 4N) [4, 11]. These granules and associated NE represent the DFz2C/LamC foci observed by light microscopy [4]. Upon expressing LamC-E174K or LamC-r564c, several common abnormalities were observed. First, megaRNPs were localized within aberrant blebs of the NE (Figures 4O, white arrow, S4H, S4M, and S4N). These blebs were limited by INM and ONM, and beneath the INM, there were areas of irregular and highly thickened lamina (Figures 4O and 4P, black arrows, and S4K). Thus, unlike the perinuclear space localization of normal megaRNPs, these granules were present in the nucleoplasm (Figures S4H and S4L). The thickened lamina was particularly prominent at the neck of the blebs (Figures 4O, black arrowhead, S4H, and S4K) but also in networks surrounding small nucleoplasmic islands (Figures 4Q, 4R, and S4J, black arrows). Additionally, blebs devoid of megaRNPs were observed at high frequency (Figure 4P, white arrowheads). These blebs most likely correspond to the blebs observed at the light microscopy level. Thus, PS-modeled mutations in LamC induce defects in NE budding. These blebs have been previously observed in HGPS cells [25], but their significance was unknown. We propose that they represent sites of aborted NE budding.

The above phenotype differed from the defects in NE budding observed in *torsin* mutants [11]. In *torsin* mutants, megaRNP granules bud into the perinuclear space but remain tethered to the INM by a "neck," as Torsin appears to be required in pinching off the INM-coated granule [11] (Figure S4L). In contrast, megaRNPs in PS-modeled LamC mutations were not surrounded by INM and remained naked in the nucleoplasmic side of the projection (Figure S4L). We propose that, in PS-modeled mutations, LamC forms a disrupted lamina network, preventing megaRNPs from accessing the INM to bud into the perinuclear space. Unlike *torsin* mutants, where megaRNP granules accumulate at the perinuclear space, very few megaRNPs were observed in PS-modeled LamC mutations. As megaRNPs are tightly surrounded by INM in *torsin* mutants, it is possible that they are protected from degradation. Instead, megaRNPs in PS-modeled mutations remain in the nucleoplasm being susceptible to degradation. This is supported by the observation that *marf* RNA is severely decreased in the LamC mutations and does not simply accumulate in the nucleus.

PS-Modeled LamC Mutations Impair NMJ Development

As another NE-budding readout, we examined the larval NMJ. Mutations in genes encoding components of NE budding result in the accumulation of immature synaptic boutons (ghost boutons) that fail to recruit postsynaptic proteins [4, 11]. This phenotype can be visualized by labeling NMJs with markers of the presynaptic (anti-HRP) and postsynaptic (anti-Discs-Large [DLG]) compartments, as ghost boutons lack DLG. We found that LamC-WT rescued the increase in ghost boutons in *lamC* mutants (Figures S4O, S4P, and S4R). In contrast, neither LamC-E174K nor LamC-r564c rescued this defect (Figures S4Q and S4R). Thus, expression of PS-modeled LamC variants results in abnormal NMJ development and mimics the effects of inhibiting NE budding. NE budding blockade was observed in the larva, which is well before any signs of aging were detected, suggesting that NE-budding defects were unlikely to be caused by accelerated aging. We propose that certain transcripts required for mitochondrial renewal are delivered from the nucleus through NE budding. Mutations blocking NE budding are initially normal but fail to maintain this cellular state, resulting in accelerated aging.

HGPS patients do not display signs of intellectual disability [26]. However, PS patients commonly have decreased NMJ performance [27], defects in the enteric nervous system [28], low-frequency conductive hearing loss, and peripheral neuropathy [29]. Thus, synaptic dysfunction in PS patients cannot be completely ruled out. Our studies reveal a new role for NE budding in aging and provide a mechanism for premature aging in certain laminopathies.

EXPERIMENTAL PROCEDURES

For detailed methods, see Supplemental Experimental Procedures.

Molecular Biology

LamC clone LD31805 was mutagenized using site-directed mutagenesis. For fly transformation, LamC constructs were subcloned into pUAST-attB.

Fly Strains

pUAST-LamC-WT, pUAST-LamC-E174K, and pUAST-LamC-R564C were integrated at P2(3L)68A4. Stocks used were CS (WT), UAS-Marf-RNAi, UAS-Blw-RNAi, UAS-Dfz2-DN, UAS-Marf-HA, $lamC^{EX296}$, $lamC^{EX265}$, and the Gal4 drivers BG487-Gal4 and MHC-Gal4.

Western Blots

Western blots were performed as in [30], with few modifications.

Immunocytochemistry

Immunocytochemistry was performed in wandering third instar body wall muscles, adult indirect flight-muscle thoraces, and S2 cells. Primary antibodies were anti-DLG_{PDZ}, anti-ubiquitin-FK2, anti-LamC, anti-ATP5A, and anti-DFz2-C.

S2 Cell Culture

S2 cell culture was generated and cultured as in [30]. Protein expression was induced with 0.7 mM $CuSO_4$ for 24 hr.

Fluorescence In Situ Hybridization

FISH was performed as in [4], with few modifications.

Image Acquisition, Quantification, and Morphometric Analysis

Image acquisition, quantification, and morphometric analysis were performed as in [4]. Polyubiquitin and mitochondrial volume were normalized to muscle volume. Number of nuclear DFz2C/LamC foci and percent of nuclei having more than ten blebs were determined from muscles 6 and 7 (A2 and A3). Number of foci per nucleus was normalized to WT controls. Mitochondrial density was measured using ImageJ.

Electron Microscopy

Electron microscopy (EM) was carried out as described in [4].

Flight Assay

Flight assay was conducted as described in [24].

RNA Immunoprecipitation

RIP was performed as described in [12], with a few modifications.

qPCR

qPCR was performed as described in [12]. mRNA levels were calculated by the $2^{\Delta Ct}$ method, where ΔCT = (DFz2C IP Ct − control IP Ct), and then normalized to Marf levels for RIP. For comparisons between genotypes, *marf* RNA levels were normalized to a reference gene, either *Ef1α48D* or *RpL32* [31], by the $2^{-\Delta Ct}$ method. RNA levels were then normalized to controls for each experiment.

Statistics

A one-way ANOVA followed by Tukey's post hoc test was utilized for multiple comparisons.

SUPPLEMENTAL INFORMATION

Supplemental Information includes four figures, Supplemental Experimental Procedures, and two movies and can be found with this article online at http://dx.doi.org/10.1016/j.cub.2016.06.007.

AUTHOR CONTRIBUTIONS

Conceptualization, V.B., J.A., and Y.L.; Methodology, Y.L. and V.B.; Validation, Y.L.; Investigation, Y.L., L.H., T.T., B.D., J.A., and W.H.; Resources, V.B., Department of Neurobiology, UMMS Electron microscopy core; Formal Analysis, Y.L., B.D., and V.B.; Visualization, V.B.; Writing – Original Draft, V.B.; Writing – Review & Editing, Y.L., J.A., and V.B.; Project Administration, Y.L. and V.B.; Funding Acquisition, V.B.; Supervision, V.B. and J.A.

ACKNOWLEDGMENTS

We thank Dr. Lee Fradkin for helpful comments on the manuscript as well as Dr. Melissa Moore and members of the V.B. lab for thoughtful discussions. We also thank the UMMS EM Facility for assistance in this project. We also thank Dr. Leo Pallanck for the UAS-Marf-HA line. Stocks obtained from the Bloomington Drosophila Stock Center (NIH P40OD018537) were used in this study. This study is supported by NIH grant R01 NS063228 to V.B.

Received: February 25, 2016
Revised: May 9, 2016
Accepted: June 3, 2016
Published: July 21, 2016

REFERENCES

1. Chandris, P., Giannouli, C.C., Panayotou, G., and Kletsas, D. (2010). Compromise in mRNA processing machinery in senescent human fibroblasts: implications for a novel potential role of Phospho-ATR (ser428). Biogerontology *11*, 421–436.
2. Cookson, M.R. (2012). Aging–RNA in development and disease. Wiley Interdiscip. Rev. RNA *3*, 133–143.
3. Dupuis, L. (2014). Mitochondrial quality control in neurodegenerative diseases. Biochimie *100*, 177–183.
4. Speese, S.D., Ashley, J., Jokhi, V., Nunnari, J., Barria, R., Li, Y., Ataman, B., Koon, A., Chang, Y.-T., Li, Q., et al. (2012). Nuclear envelope budding enables large ribonucleoprotein particle export during synaptic Wnt signaling. Cell *149*, 832–846.
5. Lee, C.P., and Chen, M.R. (2010). Escape of herpesviruses from the nucleus. Rev. Med. Virol. *20*, 214–230.
6. Demontis, F., and Perrimon, N. (2010). FOXO/4E-BP signaling in *Drosophila* muscles regulates organism-wide proteostasis during aging. Cell *143*, 813–825.
7. Rubinsztein, D.C. (2006). The roles of intracellular protein-degradation pathways in neurodegeneration. Nature *443*, 780–786.
8. Demontis, F., Piccirillo, R., Goldberg, A.L., and Perrimon, N. (2013). Mechanisms of skeletal muscle aging: insights from *Drosophila* and mammalian models. Dis. Model. Mech. *6*, 1339–1352.
9. Doran, P., Donoghue, P., O'Connell, K., Gannon, J., and Ohlendieck, K. (2009). Proteomics of skeletal muscle aging. Proteomics *9*, 989–1003.
10. Mettenleiter, T.C., Müller, F., Granzow, H., and Klupp, B.G. (2013). The way out: what we know and do not know about herpesvirus nuclear egress. Cell. Microbiol. *15*, 170–178.
11. Jokhi, V., Ashley, J., Nunnari, J., Noma, A., Ito, N., Wakabayashi-Ito, N., Moore, M.J., and Budnik, V. (2013). Torsin mediates primary envelopment of large ribonucleoprotein granules at the nuclear envelope. Cell Rep. *3*, 988–995.
12. Packard, M., Jokhi, V., Ding, B., Ruiz-Cañada, C., Ashley, J., and Budnik, V. (2015). Nucleus to synapse Nesprin1 railroad tracks direct synapse maturation through RNA localization. Neuron *86*, 1015–1028.
13. Peterson, C.M., Johannsen, D.L., and Ravussin, E. (2012). Skeletal muscle mitochondria and aging: a review. J. Aging Res. *2012*, 194821.
14. Davies, K.M., Anselmi, C., Wittig, I., Faraldo-Gómez, J.D., and Kühlbrandt, W. (2012). Structure of the yeast F1Fo-ATP synthase dimer and its role in shaping the mitochondrial cristae. Proc. Natl. Acad. Sci. USA *109*, 13602–13607.
15. Daum, B., Walter, A., Horst, A., Osiewacz, H.D., and Kühlbrandt, W. (2013). Age-dependent dissociation of ATP synthase dimers and loss of inner-membrane cristae in mitochondria. Proc. Natl. Acad. Sci. USA *110*, 15301–15306.
16. Garg, A., Subramanyam, L., Agarwal, A.K., Simha, V., Levine, B., D'Apice, M.R., Novelli, G., and Crow, Y. (2009). Atypical progeroid syndrome due to heterozygous missense LMNA mutations. J. Clin. Endocrinol. Metab. *94*, 4971–4983.
17. Liang, L., Zhang, H., and Gu, X. (2009). Homozygous LMNA mutation R527C in atypical Hutchinson-Gilford progeria syndrome: evidence for autosomal recessive inheritance. Acta Paediatr. *98*, 1365–1368.
18. Roy, S., and VijayRaghavan, K. (1999). Muscle pattern diversification in *Drosophila*: the story of imaginal myogenesis. BioEssays *21*, 486–498.
19. Li, L., Tian, X., Zhu, M., Bulgari, D., Böhme, M.A., Goettfert, F., Wichmann, C., Sigrist, S.J., Levitan, E.S., and Wu, C. (2014). *Drosophila* Syd-1, liprin-α, and protein phosphatase 2A B' subunit Wrd function in a linear pathway to prevent ectopic accumulation of synaptic materials in distal axons. J. Neurosci. *34*, 8474–8487.
20. Muchir, A., van Engelen, B.G., Lammens, M., Mislow, J.M., McNally, E., Schwartz, K., and Bonne, G. (2003). Nuclear envelope alterations in fibroblasts from LGMD1B patients carrying nonsense Y259X heterozygous or homozygous mutation in lamin A/C gene. Exp. Cell Res. *291*, 352–362.
21. Mathew, D., Ataman, B., Chen, J., Zhang, Y., Cumberledge, S., and Budnik, V. (2005). Wingless signaling at synapses is through cleavage and nuclear import of receptor DFrizzled2. Science *310*, 1344–1347.
22. Mateos, J., Landeira-Abia, A., Fafián-Labora, J.A., Fernández-Pernas, P., Lesende-Rodríguez, I., Fernández-Puente, P., Fernández-Moreno, M., Delmiro, A., Martín, M.A., Blanco, F.J., and Arufe, M.C. (2015).

iTRAQ-based analysis of progerin expression reveals mitochondrial dysfunction, reactive oxygen species accumulation and altered proteostasis. Stem Cell Res. Ther. *6*, 119.

23. Scheckhuber, C.Q., Erjavec, N., Tinazli, A., Hamann, A., Nyström, T., and Osiewacz, H.D. (2007). Reducing mitochondrial fission results in increased life span and fitness of two fungal ageing models. Nat. Cell Biol. *9*, 99–105.
24. Benzer, S. (1973). Genetic dissection of behavior. Sci. Am. *229*, 24–37.
25. Kandert, S., Lüke, Y., Kleinhenz, T., Neumann, S., Lu, W., Jaeger, V.M., Munck, M., Wehnert, M., Müller, C.R., Zhou, Z., et al. (2007). Nesprin-2 giant safeguards nuclear envelope architecture in LMNA S143F progeria cells. Hum. Mol. Genet. *16*, 2944–2959.
26. Nissan, X., Blondel, S., Navarro, C., Maury, Y., Denis, C., Girard, M., Martinat, C., De Sandre-Giovannoli, A., Levy, N., and Peschanski, M. (2012). Unique preservation of neural cells in Hutchinson- Gilford progeria syndrome is due to the expression of the neural-specific miR-9 microRNA. Cell Rep. *2*, 1–9.
27. Greising, S.M., Call, J.A., Lund, T.C., Blazar, B.R., Tolar, J., and Lowe, D.A. (2012). Skeletal muscle contractile function and neuromuscular performance in Zmpste24 -/- mice, a murine model of human progeria. Age (Dordr.) *34*, 805–819.
28. Yang, S.H., Procaccia, S., Jung, H.J., Nobumori, C., Tatar, A., Tu, Y., Bayguinov, Y.R., Hwang, S.J., Tran, D., Ward, S.M., et al. (2015). Mice that express farnesylated versions of prelamin A in neurons develop achalasia. Hum. Mol. Genet. *24*, 2826–2840.
29. Goss, J.R., Stolz, D.B., Robinson, A.R., Zhang, M., Arbujas, N., Robbins, P.D., Glorioso, J.C., and Niedernhofer, L.J. (2011). Premature aging-related peripheral neuropathy in a mouse model of progeria. Mech. Ageing Dev. *132*, 437–442.
30. Koles, K., Nunnari, J., Korkut, C., Barria, R., Brewer, C., Li, Y., Leszyk, J., Zhang, B., and Budnik, V. (2012). Mechanism of evenness interrupted (Evi)-exosome release at synaptic boutons. J. Biol. Chem. *287*, 16820–16834.
31. Ling, D., and Salvaterra, P.M. (2011). Robust RT-qPCR data normalization: validation and selection of internal reference genes during post-experimental data analysis. PLoS ONE *6*, e17762.